Journal of Materials Chemistry A

Accepted Manuscript

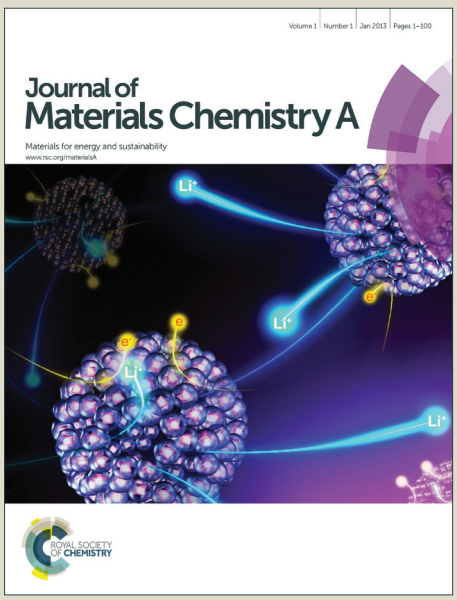

ROYAL SOCIETY OF CHEMISTRY

www.rsc.org/materialsA

Electrospun NiO nanofibers as cathode materials for high performance asymmetric supercapacitors

Muhamed Shareef Kolathodi, Milan Palei and Tirupattur Srinivasan Natarajan*

Conducting Polymer Lab, Department of Physics, Indian Institute of Technology Madras, Chennai - 600036, India Fax: +91- 44 22574852; Tel: +91- 4422574860;

**Corresponding Author: tsn@iitm.ac.in*

Abstract

Asymmetric supercapacitors (ASC) based on aqueous electrolytes got wide attention in energy research in recent years due to high energy and power densities achievable in addition to being 'green electrolyte'. Herein, we report an ASC built with electrospun nanofibers of NiO as battery type cathode material and commercially available high surface area activated carbon as capacitor type anode material with appropriate mass loadings. We synthesized high aspect ratio nanofibers of NiO by simple and cost effective sol-gel based electrospinning followed by annealing. In the end these nanofibers were composed of densely packed hexagonal nanoparticles of polycrystalline NiO having diameters ~15 nm. The ASC was capable of operating in the potential window 1.5 V in 6 M KOH solution with a gravimetric capacitance of 141 Fg^{-1} and energy density of 43.75 Wh kg^{-1}. The ASC showed high retention in the specific capacitance for 5000 galvanostatic charge discharge cycles with improved coulombic efficiency.

Introduction

Research into electrochemical energy conversion and storage devices attracts wide attention due to the rapid depletion of fossil fuels. Supercapacitor (SC) can be used for energy storage due to its higher energy density compared to conventional capacitor and higher power density and cycle stability as compared to

batteries.[1-4] However, use of SCs for practical applications is limited by the lower energy density compared to batteries. This can be overcome by widening the cell voltage and improving specific capacitance (Energy = ½ CV^2).[5] The cell voltage can be increased by using electrolytes such as organic electrolytes and ionic liquids having higher potential window.[6-9] But it is highly advantageous to use aqueous electrolytes for SCs due to their environmental benignity, cost effectiveness, high ionic conductivity and easiness of handling as compared to non-aqueous electrolytes in addition to their high specific capacitance.[10,11] Again, the voltage window can be broadened by designing asymmetric SCs (ASC) using battery type Faradaic electrode which act as energy source and capacitive electrode which act as power source; both having different potential windows which accounts for the widened cell voltage.[12-14]

Based on the energy storage mechanism, SCs can be classified into two types: (i) carbon materials based electric double layer capacitor (EDLC) (ii) transition metal oxide (TMO) and conducting polymer based redox supercapacitor, also known as pseudocapacitor. EDLC stores charges at the electrode electrolyte interface by means of charge separation while pseudocapacitor stores the electric charge by fast and reversible redox reactions on the surface or near the surface. Pseudocapacitors have higher specific capacitance and energy density while carbonaceous double layer capacitors have higher electrochemical stability.[1,2,13,15] Among the TMOs, Nickel oxide (NiO) nanostructure got wide attention for supercapacitor applications due to its high theoretical specific capacitance (~ 2573 Fg^{-1} within 0.5 V) in addition to cost effectiveness, eco-friendly nature and low toxicity.[16-18] However, the poor electric conductivity and lack of stability reduces its usage in the pristine form for practical supercapacitor applications. Therefore hybrid configuration of NiO in combination with carbon materials can be

considered for SC electrodes due to the synergic contribution of NiO and carbon materials.[19-21] A wide spectrum of NiO nanostructures can be prepared by different means such as solvothermal, hydrothermal, precipitation, solgel method etc.[20-23] Electrospinning got wide attention as compared to others due to its simple, versatile and cost effective approach.[24-26] Electrospun metal oxide nanofibers are characterized by granular and fibrous morphology, high aspect ratio and large surface to volume ratio, high crystallinity and improved mechanical strength, which makes them ideal candidate for energy storage and conversion applications such as solar cells, lithium-ion batteries, fuel cells and supercapacitors. The nanofibrous morphology creates an easy path for the electron transport and thus improves the energy storage.[27-30]

There are only a few reports in the literature on the design and development of ASCs based on NiO nanostructures. It has been reported that the ASC based on hierarchical porous NiO and carbon electrodes could operate in the potential window 0 to 1.5 V.[31] Wang et al. reported an ASC using NiO grown on graphene foam as anode and hierarchical porous nitrogen doped carbon nanotubes as cathode via complex pulsed laser deposition technique using ozone as oxidant.[32] Yuan et al. studied the temperature effect on a gel electrolyte based ASC designed with NiO and activated carbon as electrodes.[33] An ASC developed using NiO as positive electrode and $Ru_{0.35}V_{0.65}O_2$ as negative electrode could operate at 1.7 V.[34] Recently, Luan et al. reported an ASC on a carbon fiber cloth using nickel oxide nanoflake arrays and reduced graphene oxide as electrodes.[35] In this paper, we report the preparation of highly crystalline and high aspect ratio nanofibers of NiO by annealing an electrospun membrane of nickel acetate-poly(vinylpyrrolidone) composite. An ASC was developed using 6 M KOH electrolyte with a battery type Faradaic electrode made of NiO nanofibers and high surface area activated carbon

composite while the capacitive type electrode was made from activated carbon. To the best of our knowledge an ASC based on electrospun NiO NFs is being reported for the first time.

2. Experimental section

2.1 Preparation of NiO nanofibers

All the chemicals used were of analytical grade and used as received without further treatment. Nickel acetate $(CH_3COO)_2Ni{\cdot}4H_2O$; (here onwards referred to as NiAc), ethanol and dimethylformamide (DMF) were purchased from Merck (India) Ltd. Poly(vinylpyrrolidone) (PVP, Molecular weight 1,300,000) and activated carbon (AC, surface area ~ 2200 m^2g^{-1}) were obtained from Alfa Aesar and Kuraray Chemical respectively. Poly(vinylidene fluoride) (PVDF) and N-methylpyrrolidinone (NMP) were purchased from Sigma-Aldrich. In a typical procedure, a known amount of PVP was well dispersed in ethanol by stirring overnight. To this PVP dispersion, a pre synthesized NiAc solution (in DMF and ethanol) was added and kept for overnight stirring (The experimental details are reported in the Table S1 of supporting information). As-prepared NiAc-PVP sol-gel is used in an electrospinning apparatus (PICO India) at an electric potential of 20 kV with a feed rate of 1 mL/h. Fig. S1 in supporting information shows the schematic of the electrospinning set up. As-spun fibers were collected on an aluminium substrate kept at 15 cm away from the syringe tip. Afterwards, the as-spun fibers were subjected to calcination at 600 °C for 3 h with a heating rate of 2 °C/min which resulted in the formation of NiO nanofibers (NiO NFs).

2.2 Characterization of NiO nanofibers

Various spectroscopic and microscopic analyses were carried out for the characterization of as-spun NiAc-PVP NFs and annealed NiO NFs in addition to

the X-ray diffraction and thermal analysis. Powder X-ray diffraction patterns were recorded with PANalytical X'pert Pro diffractometer which was equipped with nickel-filtered Cu K_α radiation having wavelength 1.54 Å. The patterns were collected over a range of 20° - 85° in steps of 0.016° per second at room temperature. Raman spectrum of the NiO NFs was recorded using Horiba Jobin Yvon HR 800 which was equipped with optical microscope and 100x objective lens for a total magnification of 1000. The spectral resolution of the spectrometer was 2 cm^{-1} and the Raman signals were excited by Helium Neon laser of wavelength 632.8 nm. Thermogravimetric analysis (TGA, SDT Q600 TA) was conducted under nitrogen atmosphere in the temperature range of 30°-800 °C at a heating rate of 20 °C min^{-1}. The morphology of the nanofibers was observed with field emission scanning electron microscope (FEI Quanta FEG 400) at an accelerating voltage of 15 kV and transmission electron microscope (Philips CM20 TEM at 200 kV) equipped with an energy dispersive X-ray spectrometer. The exact mass of the electrode materials were obtained with a METTLER TOLEDO XS105 analytical balance having a readability of 0.01 mg.

2.3 Electrochemical Measurements

ASC was designed from two different types of electrodes; capacitive type negative electrode from commercially purchased activated carbon (AC) and battery type positive electrode from a composite of activated carbon and NiO NFs (NiO-AC) on Toray carbon paper. Electrochemical properties of the prepared electrode (NiO-AC) to execute as cathode material for the ASC was performed at room temperature using three electrode set up in 6 M KOH solution. A platinum wire and saturated silver/silver chloride (Ag/AgCl) served as counter and reference electrodes respectively. In order to design ASC, positive electrode was prepared by dispersing NiO NFs, AC and PVDF in NMP in the weight ratio of 70:25:5 and

negative electrode was prepared from AC and PVDF in the ratio 95:5 by weight. The electrode materials were brush coated on Toray carbon papers and dried at 60 °C overnight. Since NiO is stable in KOH solution as compared to neutral and acidic electrolytes, 6 M aqueous KOH solution is used as electrolyte. Whatman filter paper soaked in 6 M KOH solution is used as separator with stainless steel plates as current collectors. Electrochemical studies of the ASC were investigated with two electrode set up using potentiostat (Ivium Compact Stat, Ivium technologies) at room temperature. The cyclic voltammetry (CV) and galvanostatic charge-discharge (GCD) cycles were performed in the potential window 0 to 1.5 V. Electrochemical impedance spectrum (EIS) of the device was carried out with an alternating voltage of amplitude 5 mV, in the frequency range of 100 kHz to 0.1 Hz under open circuit condition.

3. Results and Discussion

Fig. 1(a) shows the typical XRD pattern of NiO NFs. Fig. S2, in supporting information shows the XRD pattern of as-spun NiAc-PVP Nanofibers. All the diffraction peaks could be assigned to a single phase of face centered cubic (FCC) phase NiO (JCPDS card no. #47-1049, a = 4.177 Å). The absence of peaks in XRD corresponding to other phases of NiO or oxides of Ni confirmed the purity of annealed sample. The sharper peaks are indicative of high crystallinity of the NiO NFs. The more intense peak located at $2\theta = 43.3°$ indicates that crystal growth is dominated through (2 0 0) plane, which corresponds to the interplanar spacing d_{200} = 0.2 nm. The average crystallite size of NiO NF was calculated using the Scherrer equation based on the (2 0 0) peak to be about 10.65 nm.

The crystalline nature of NiO NFs was further supported by confocal Raman spectroscopy analysis which is shown in fig. 1(b). The peak located at 382 cm^{-1} could be attributed to the intra-3d transition of Ni^{2+} in the NiO nanostructure and

its comparable counterpart in bulk NiO is located at 484 cm^{-1}.[36] This shift confirms the nanostructure of the NiO where the energy levels are quantum confined laterally and differ from the bulk materials. The intense peak located at 505 cm^{-1} could be assigned to NiO stretching mode and can be described as first order transverse optical phonon mode (1PTO) of NiO NFs. The peaks recorded at 708 cm^{-1} and 1064 cm^{-1} could be assigned to the second order transverse optical phonon mode (2PTO) and second order longitudinal optical phonon mode (2PLO) mode of NiO nanofiber.[37,38]

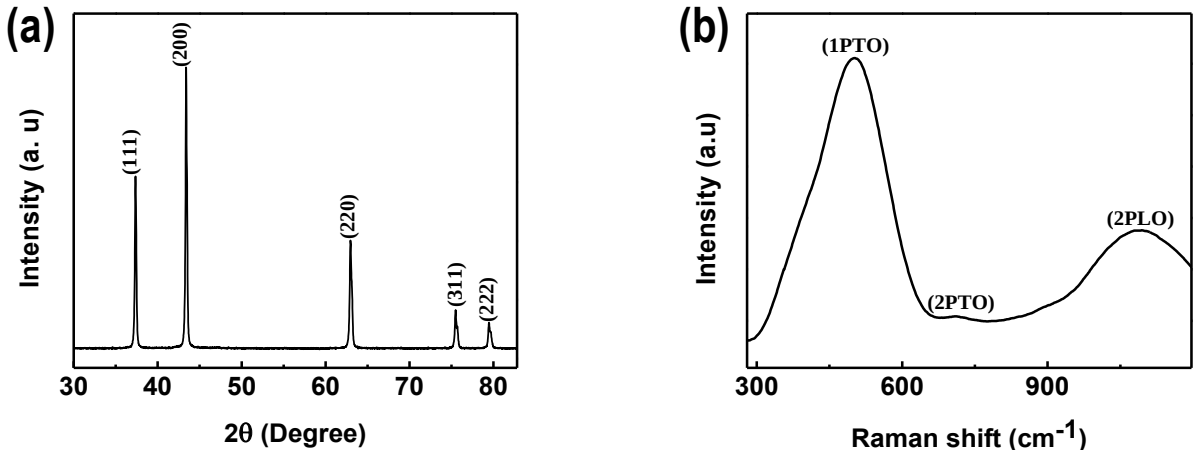

Fig. 1 (a) Powder X-Ray diffraction pattern of nickel oxide nanofibers obtained after annealing nickel acetate – PVP electrospun fibers at 600° C. All the peaks could be indexed to FCC phase of NiO (JCPDS card no. #47-1049); (b) Raman spectrum of NiO nanofibers shows the first order and second order transverse optical phonon mode as well as second order longitudinal optical phonon mode.

Fig. 2(a) shows the TGA and DSC plots of as-spun composite fibers of NiAc-PVP. As control experiment, TGA and DSC of pure PVP nanofibers were also performed and plotted in fig. 2(b). The decomposition of NiAc-PVP takes place in three steps while for pure PVP it is in two steps. For PVP, the initial weight loss (~ 9%) under 83 °C corresponds to the evaporation of solvents such as water and ethanol present in the PVP nanofibers. The relatively flat portion in the

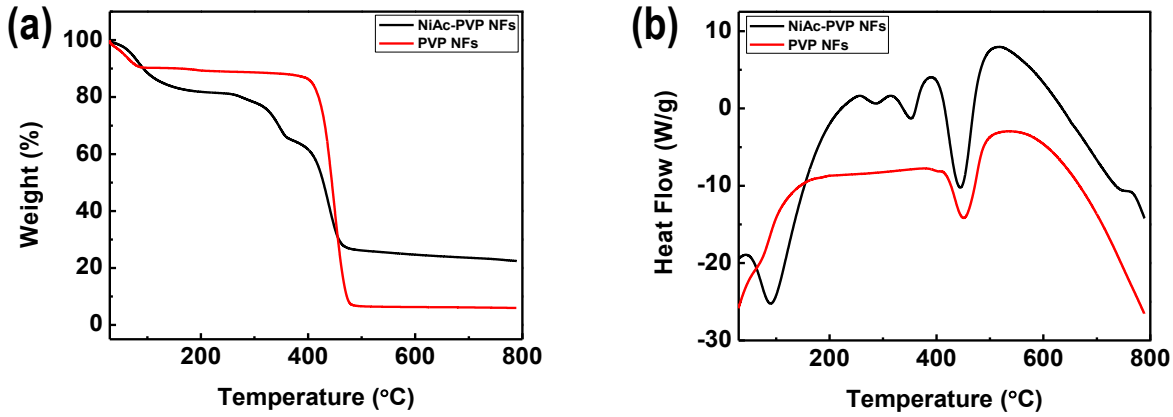

Fig. 2 Thermo gravimetric plots (a) and Differential scanning calorimetry plots (b) of as-spun NiAc-PVP nanofibers and PVP nanofibers. The complete polymer evaporation and formation of NiO occurred below 500 °C ensures that 600 °C is suitable temperature for annealing the as-spun NiAc-PVP fibers.

temperature range 85 – 383 °C of PVP indicates the slow intramolecular decomposition of PVP while the rapid weight loss started at 385 °C corresponds to the intermolecular decomposition and evaporation of PVP. The flat portion after 480 °C corresponds to the complete elimination of PVP, which is supported by the two peaks in the temperatures 61 °C and 450 °C in the DSC curve.[39] In the case of NiAc-PVP as-spun fibers, the initial weight loss (~18%) in the temperature range 60 - 130 °C could be ascribed to the evaporation of solvents and partial decomposition (melt) of NiAc with the dehydration of crystal water from NiAc. Additional weight loss in the temperature range 260 - 370 °C could be attributed to the complete dehydration and decomposition of NiAc with formation of NiO; the intramolecular decomposition of PVP as well accompanied during this temperature.[40,41] The DSC plots further support the TGA analysis, the two endothermic peaks at 68 °C confirms the removal of solvents (such as water and ethanol) and the peak at 450 °C corresponds to the decomposition of PVP. In the case of composite fibers, sharp peak located at 89.6 °C corresponds to the melting of NiAc with the removal of solvents, and the additional endothermic peaks

located at 286 °C and 350 °C correspond to the dehydration and decomposition of NiAc. It can be concluded from thermal analysis that 600 °C is the suitable temperature for the formation of NiO from NiAc via annealing.

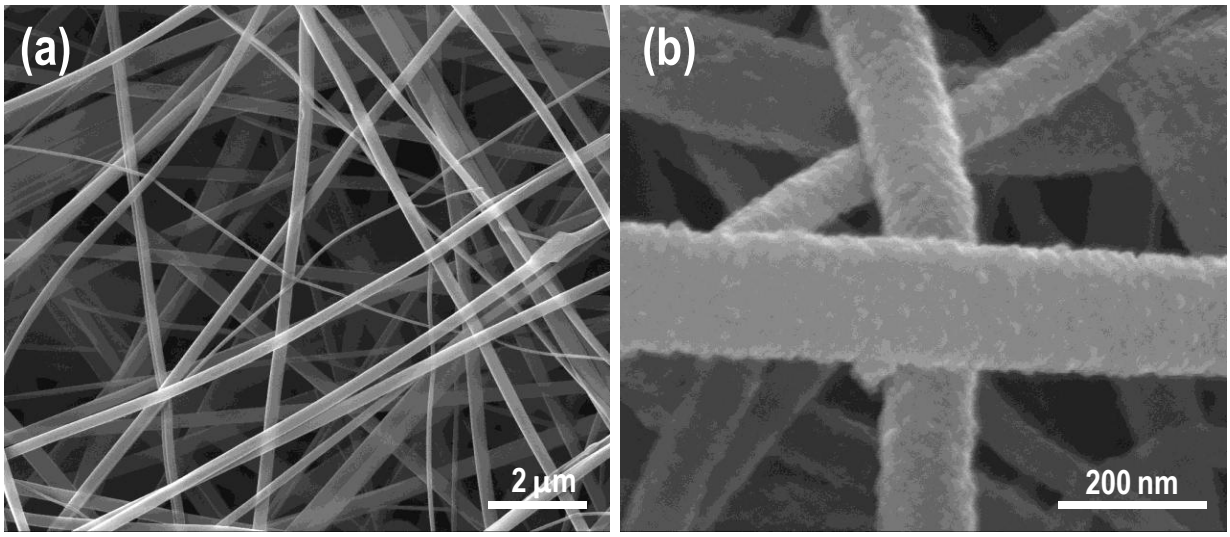

Fig. 3 Field emission scanning electron microscopic images of (a) smooth and randomly oriented as-spun NiAc-PVP fibers (300-500 nm) and (b) annealed and granulated NiO nanofibers (50-150 nm).

Figure 3(a) and 3(b) show the typical field emission scanning electron microscopy (FESEM) images of the as-spun NiAc-PVP and calcined NiO NFs. Fig. S3 and S4 show the photographic and optical microscopic images of as-spun NiAc-PVP fibers. It can be observed that the diameter of as-spun and annealed fibers vary in the range 300 - 500 nm and 50 - 200 nm respectively. As-spun fibers were randomly distributed with web like morphology and having high aspect ratio. This could be explained due to the bending instabilities and the partial evaporation of solvents, namely, water and ethanol which were linked through hydrogen bonding.[24-26] The annealed fibers were however no longer smooth and continuous but rough and thinner as compared to as-spun nanofibers due to the decomposition of polymer template and other organic parts during annealing at 600 °C.[27-30]

Furthermore, it is evident from the careful investigation of FESEM image that the annealed fibers are made of a large number of interconnected nanograins.

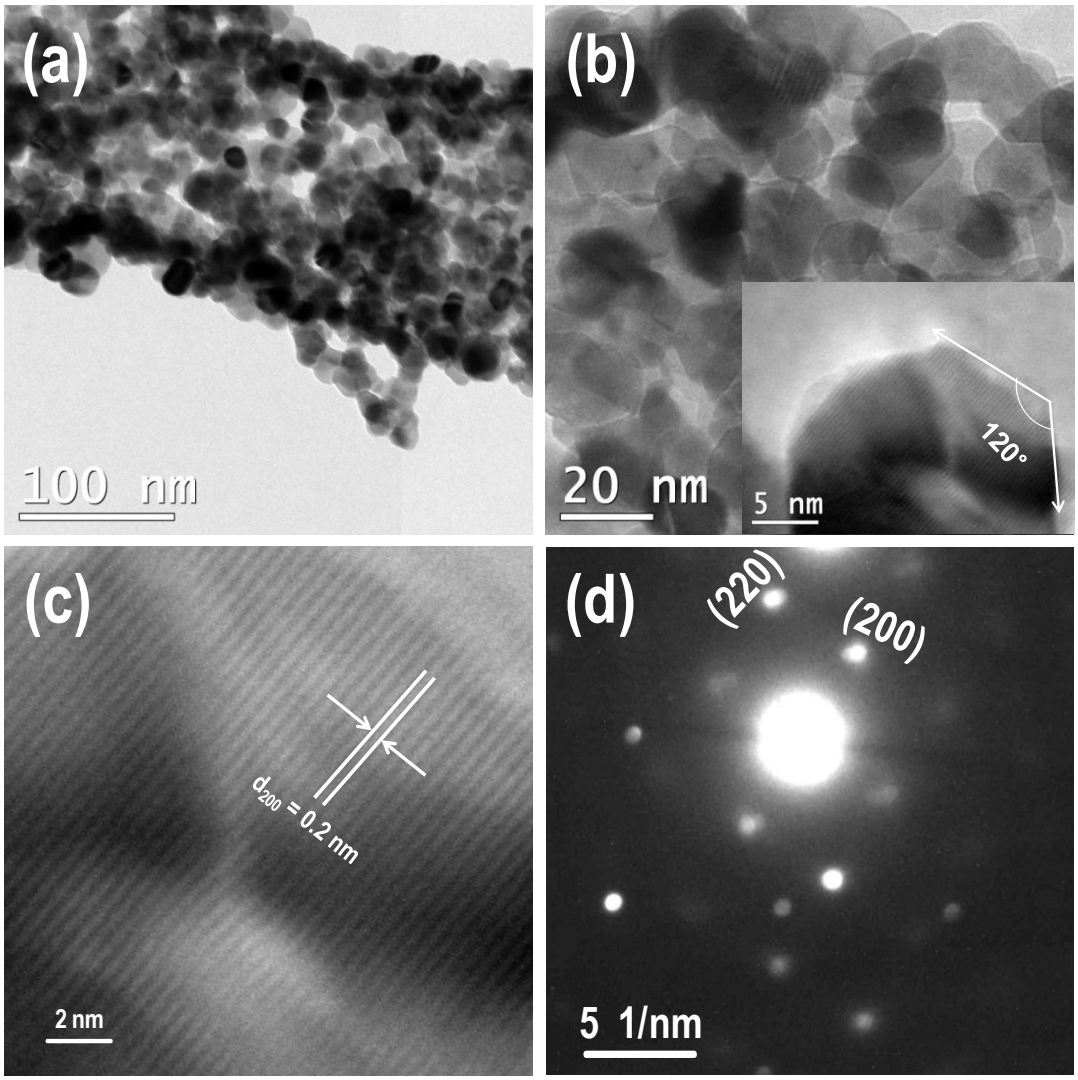

Fig. 4 (a) and (b) TEM image of NiO nanofiber; Each fibers are composed of a large number of hexagonal and quasi hexagonal particles, the edge angle is 120° as shown in the inset of fig. 4(b); (c) Lattice resolved HRTEM image shows the d spacing of 0.2 nm and (d) SAED pattern shows the polycrystalline nature of NiO nanoparticle.

The texture and crystal structure of NiO NFs were further analyzed by HRTEM images supported by selected area electron diffraction (SAED) pattern (Fig. 4(a)-(d)). Diameters of annealed fibers are of the order of 100 nm as displayed in FESEM image. Careful investigation from HRTEM image shows that NiO NFs are composed of a large number of hexagonal and quasi hexagonal

nanoparticles with an edge angle of 120° (see inset in fig. 4(b)). These NiO nanoparticles are highly crystalline in nature as revealed by well resolved lattice fringes of HRTEM image (shown in fig. 4(c)) where the crystal growth occurred along (1 1 1) plane with the interplanar spacing (d = 0.24 nm). The SAED pattern shown in fig. 4(d) indicates the polycrystalline nature of NiO nanoparticles and the sharp diffraction spots could be indexed to (2 0 0) and (2 2 0) atomic planes of face centered cubic (FCC) phase of NiO, which further supports the XRD analysis.

Electrochemical characterization

Fig. 5(a) shows the typical CV plots of the NiO-AC composite electrode recorded in the potential window 0-0.5 V at scan rates 2, 5, 10, 20 and 50 mV/s. The CV curves displayed the prevailing pseudocapacitance behavior, in addition to the double layer effect. These distorted and complex CV curves of NiO-AC electrode arises due to the double layer effect of AC and Faradic redox reaction of NiO NFs. This corresponds to oxidation and reduction peaks in the CV plot (for a scan rate of 5 mV/s) located at 0.35 V and 0.22 V respectively. The pseudocapacitive oxidation reduction performance of the NiO can be represented as

$$\mathbf{NiO + OH^- \leftrightarrow NiOOH + e^-}$$

The narrow redox peak separation indicates the excellent electrochemical reversibility of the NiO-AC electrode and the separation got widened with the gradual increase of scan rate. The plateau below 0.25 V belongs to the double layer contribution of AC. Furthermore, the galvanostatic charge discharges of the prepared NiO-AC composite electrode against Ag/AgCl electrode were investigated at current densities of 1, 2, 5 and 10 A/g in 6 M KOH solution and plotted in fig. 5(b). During galvanostatic charging, the potential increases rapidly and reaches a plateau at 0.4 V followed by slow charging until reaches its maxima.

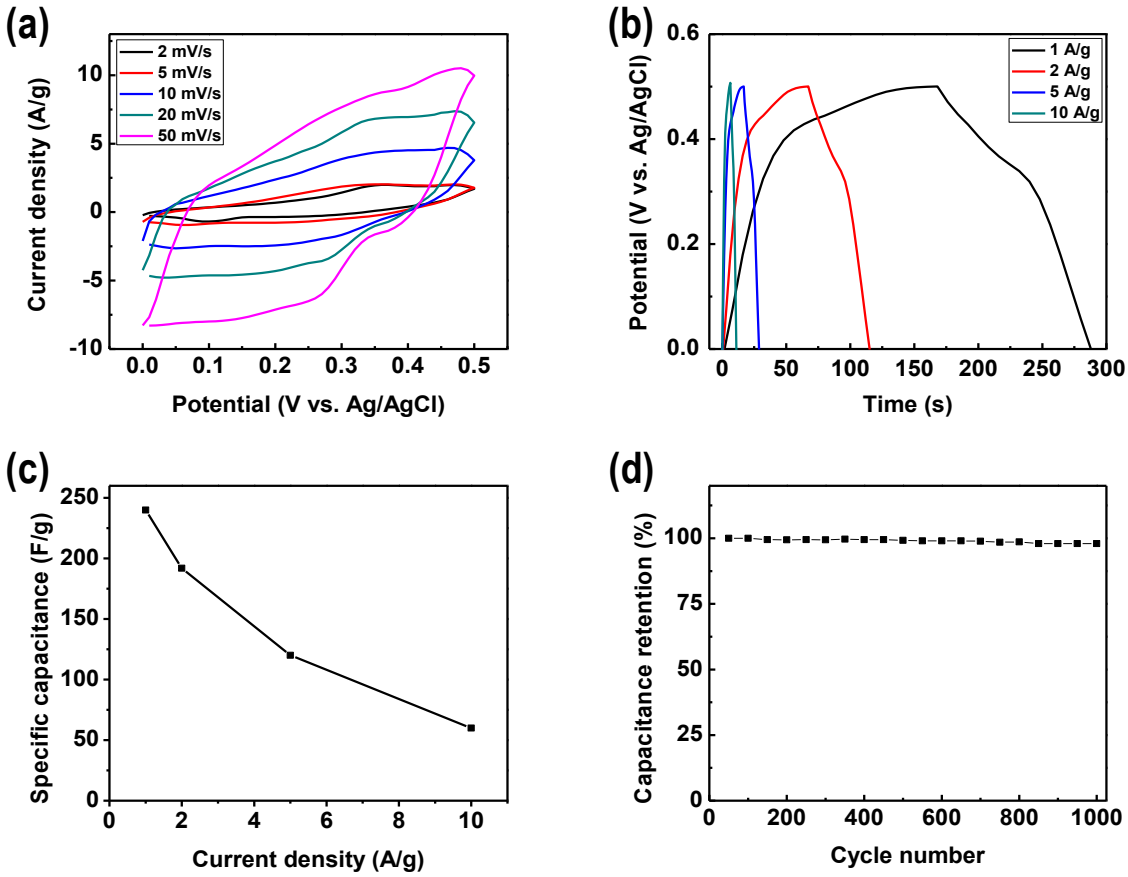

Fig. 5 Electrochemical characterization of NiO-AC NFs cathode against Ag/AgCl electrode (a) CV plots collected at scan rates of 2 - 50 mVs^{-1}; (b) Galvanostatic charging discharging plots collected at current densities of 1 – 10 Ag^{-1}; (c) Variation of specific capacitance as a function of current density; (d) Capacitance retention for 1000 galvanostatic charging discharging (GCD) cycles performed at a current density of 5 Ag^{-1}.

Similarly, during discharging the potential reduces slowly with a relatively rapid discharge at 0.35 V. The non-linear curves further revealed the pseudocapacitive behaviors of NiO and supported CV plot. The symmetric plots demonstrate excellent reversibility and coulombic efficiency of the NiO-AC electrode. The specific capacitance (C_s) of the NiO-AC electrode was estimated from the formula,

$$C_s = \frac{I\Delta t}{\Delta V} \qquad (1)$$

where I is the current density (A/g), Δt is the time of discharge (s) and ΔV is the potential window (V). The estimated specific capacitance is 248 F/g at a current

density of 1 A/g. The appreciable electrochemical performance of NiO-AC NFs justifies its selection for cathode material for ASC. Electrospun metal oxide nanofibers obtained after sintering at higher temperature resulted in highly crystalline and fibrous morphology having more electroactive surface area which enhances the pseudocapacitance. Additionally, the tightly packed polycrystalline hexagonal and quasi hexagonal nanoparticles which provide granular morphology of NiO NFs greatly improve the specific capacitance. The NiO-AC electrode exhibits specific capacitances of 182, 125 and 98 F/g at current densities of 2, 5 and 10 A/g, respectively. Fig. 5(c) shows the variation of specific capacitance with current densities. The NiO-AC electrode has subjected to 5000 charging discharging cycles at a current density of 2 A/g and found to show specific capacitance retention of 98.2 % (see fig. 5(d)).

To assemble an asymmetric supercapacitor with highest specific capacitance, charge balance ($Q^+ = Q^-$) should be maintained in both of the electrodes of ASC. Fig. 6(a) show the typical CV plots of the individual electrodes (AC and NiO-AC) recorded at a scan rate of 10 mV/s in the potential windows 0 to -1 V and 0 to 0.5 V respectively, against Ag/AgCl electrode. The rectangular shaped CV curve of activated carbon electrode displays the electric double layer capacitance while distorted CV curve of NiO-AC reveals the pseudocapacitance behavior in addition to the double layer effect. Since AC and NiO-AC can store electric charges in the potential window -1.0 V and 0.5 V vs. Ag/AgCl, respectively, the ASC designed from these electrodes, could operate from 0 to 1.5 V. Since maximum achievable potential windows of the electrodes using unit masses are estimated from the corresponding CV plots, the appropriate mass loadings of the electrode materials for designing ASC with highest performance are determined from GCD curve (see fig. S5 in SI) according to the equation[34]

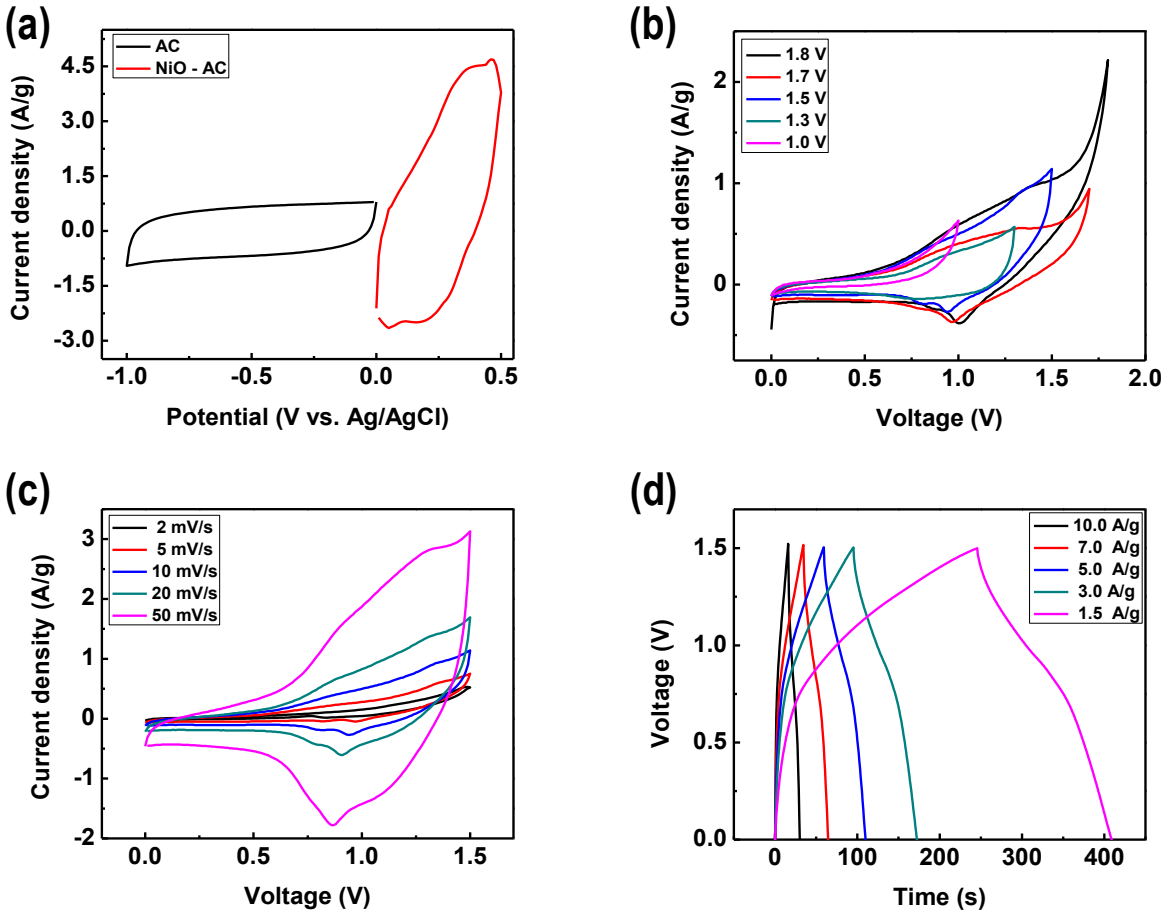

Fig. 6 Electrochemical properties of the assembled asymmetric supercapacitor AC‖AC- NiO NFs with 6 M KOH as electrolyte (a) CV plots of negative electrode activated carbon and positive electrode NiO-AC NFs at a scan rate of 10 mV/s in 6 M KOH electrolyte; (b) CV plots recorded at a scan rate of 10 mV/s for different voltage windows; (c) CV plots of the ASC recorded at different scan rates; (d) Galvanostatic charge discharge plots recorded at different current densities.

$$\frac{m_+}{m_-} = \frac{C_{s-} \times V_-}{C_{s+} \times V_+} \qquad (2)$$

where Q^+ and Q^- are the charges of positive and negative electrodes of the ASC having masses of m_+ and m_-, respectively. The specific capacitances of the electrode materials are C_{s+} and C_{s-} at potential windows of V_+ and V_- when measured with three electrode set up. Specific capacitances of the electrode materials were estimated from the GCD plots according to the equation (1). Mass loading ratio of positive and negative electrodes in the ASC could be estimated to

1.076 according to the equation (2), so that 0.5 mg of negative electrode (AC) and 0.576 mg of positive electrode (NiO-AC) were used in order to maintain the charge neutrality of ASC. The electrochemical calculations were carried out based on the total mass of electrode materials in the ASC. After determining the potential windows of each electrode materials, an asymmetric supercapacitor (ASC) was designed using AC as anode and NiO-AC NFs as cathode. Fig. 6(b) show the cyclic voltammograms of the designed ASC recorded at a scan rate of 10 mV/s with different voltage windows. It is observed from the CV plots shown in fig. 6(b) that the ASC could be operated till 1.8 V at a scan rate of 10 mV/s. But during slow scan rates such as 1 and 2 mV/s, the current increases rapidly until it reaches the breakdown point of electrolyte at higher voltage windows 1.7 V and 1.8 V. Therefore, for the sake of safety and long life of ASC, it is highly recommended to operate up to 1.5 V. Fig. 6(c) show the CV curves of the ASC plotted in the voltage window 0 to 1.5 V at scan rates of 2, 5, 10, 20 and 50 mV/s. All the CV plots are similar in shape with maintaining a pair of cathodic and anodic peaks. These redox peaks in the CV plots got shifted away from each other as the scan rates goes higher. The redox peaks are indicative of pseudocapacitive nature of the ASC and are dominated enormously over the double layer contribution of AC which was very clear from the large area of corresponding CV plots. CD curves of the ASC are plotted in fig. 6(d) at current densities of 1.5, 3, 5, 7 and 10 A/g within the voltage window 0 to 1.5 V. The nonlinear CD plots further supports the fast and reversible redox peaks recorded in the CV plots.

The specific capacitance (C_s), energy density (E_s) and power density (P_s) of the ASC (expressed in Fg^{-1}, Wh kg^{-1} and kW kg^{-1}, respectively) were calculated from GCD curve according to the formulae

$$C_s = \frac{I\Delta t}{m\Delta V} \quad (3)$$

$$E_s = \frac{C_s \Delta V^2}{7.2} \quad (4)$$

$$P_s = \frac{3.6E_s}{t} \quad (5)$$

Where I is the current density (A/g), Δt is the time of discharge (s), m is the total mass in both of the electrodes (g) and ΔV is the potential window (V). Specific capacitances at different current densities were estimated and plotted in fig. 7(a). The highest value of specific capacitance, 141 F/g, was achieved at a current density of 1 A/g, with a gradual reduction to 93 F/g at a current density of 10 A/g. The estimated specific capacitance, energy density and power density of the designed ASC was compared with previously reported ASCs based on different NiO structures and shown in the table 1. Ragone plot of the ASC (E_s vs. P_s) is shown in fig. 7(b). The cyclic stability of a supercapacitor determines its application in industry. Here the designed ASC has been subjected to 5000 galvanostatic charging discharging cycles at a current density of 10 A/g. The capacitance retention and coulombic efficiency of the ASC are plotted in fig. 7(c). The last five cycles of the GCD curves are plotted in fig. 7(d) and the initial five cycles are shown in fig. S6 of supporting information for comparison. It has been found that ASC retains its specific capacitance by 88% with improving the coulombic efficiency ($\eta = t_d/t_c \times 100$) higher than the initial cycles (88% to 93%). The excellent specific capacitance, cyclic stability performance and columbic efficiency of the ASC could be attributed to the high surface area of AC and well crystallized granular fibers of NiO nanoparticles. The dominated

pseudocapacitance of NiO NFs as revealed from the CV plots over the double layer effect of AC could be substantiated by its unique structure. The granulated nanofibers of NiO provide a large ion accessible surface for the ion diffusion and insertion-desertion. Moreover the well assembled composite nature of NiO and highly conductive AC facilitates the electronic charge transport between poorly conducting NiO and the current collector.

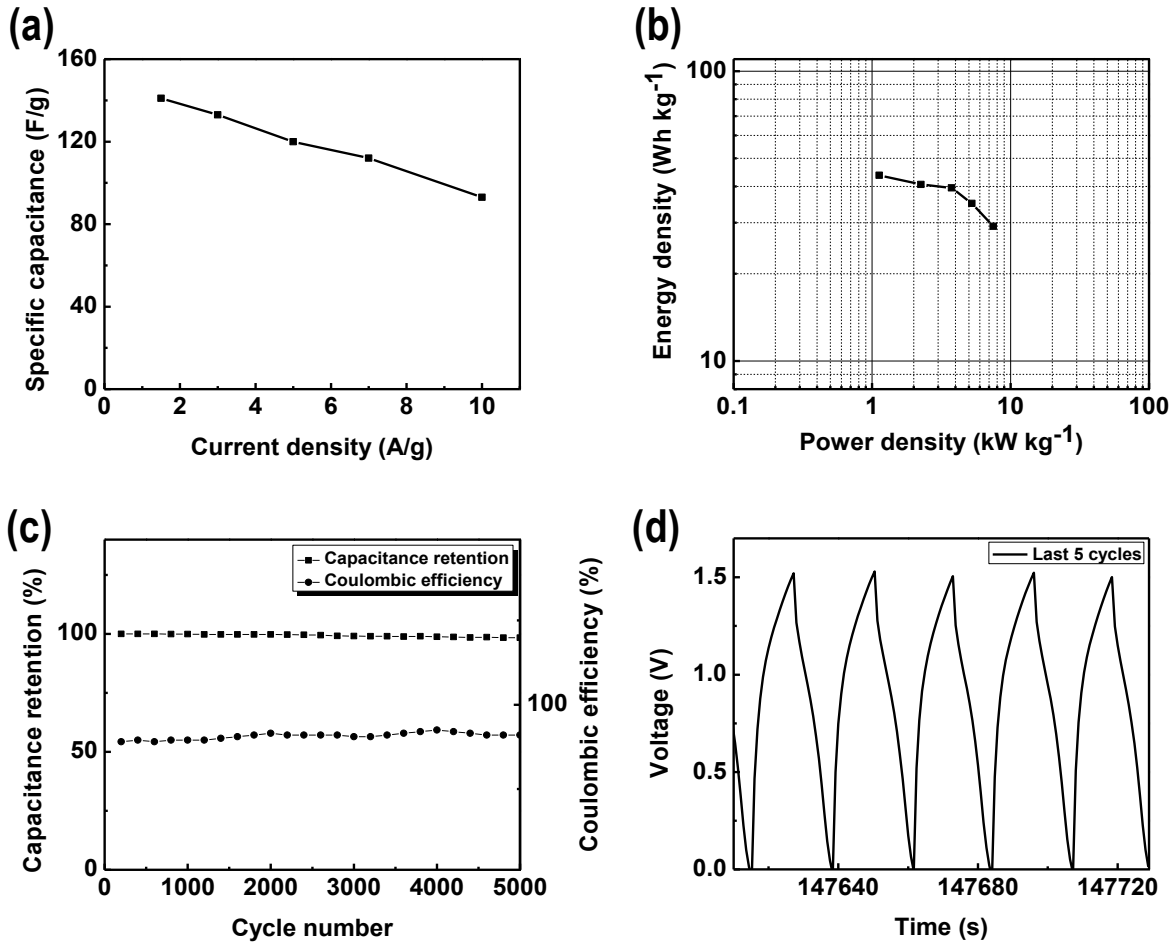

Fig. 7. Performance of the designed ASC based on AC‖AC- NiO NFs. (a) Specific capacitance as a function of current density; (b) Ragone plot of the supercapacitor (energy density vs. power density); (c) Capacitance retention and coulombic efficiency for 5000 galvanostatic charge discharge cycles carried out at a current density of 10 A/g; (d) Last five cycles of the 5000 continuous galvanostatic charge discharge cycles.

Further electrochemical analysis for determining the internal resistance and charge transport of the ASC was performed with electrochemical impedance

spectroscopy. Fig. 8(a) shows the Nyquist plot of the ASC in the frequency range 100 kHz-0.1 Hz with a signal amplitude of 5 mV under open circuit potential (OCP). The EIS plot could be easily distinguishable into a distorted semicircle at high frequency region and a straight line with a slope towards low frequency region. The semicircle represents the charge transfer process and the sloped line represents the capacitive nature of the device. The equivalent series resistance (ESR) could be estimated from the intercept at real impedance axis is found to be 6.3 Ω which constitutes the resistance of the electrolyte, resistance at electrode electrolyte interface, internal resistance of the electrode material and the contact resistance between electrode and current collector. The diameter of the semicircle reveals the charge transfer resistance (R_{ct}). The impedance spectrum was fitted with Randles equivalent circuit as shown in the inset of fig. 8(b) which consists of bulk solution resistance (R_s), charge transfer resistance (R_{ct}), Warburg impedance related to the electrolyte ion diffusion (Z_w), double layer capacitance (C_{dl}) and pseudocapacitance (C_p) and the values for R_s and R_{ct} estimated from the equivalent circuit are 6.2 Ω and 6.4 Ω, respectively. The lower value of R_{ct} could be attributed to the appreciable interfacial conductivity of NiO nanoparticles of size 15 nm and higher surface area of the activated carbon. The large slope in low frequency region of the Nyquist plot could be ascribed to the Warburg behavior which arose from the fast ion diffusion across the electrode electrolyte interface. Fig. 8(b) and 8(c) represent the bode plots of phase angle and bode plot of impedance against frequency for the ASC. The phase angle 72° at low frequency corresponds to capacitance contribution from both double layer capacitance and pseudocapacitance. The energy losses in the ASC by irreversible process could be identified from the imaginary part of the capacitance which is shown in fig. 8(d) and can be estimated according to the equation[42]

$$C'' = \frac{Z'(\omega)}{\omega |Z(\omega)|^2} \qquad (6)$$

where $Z'(\omega)$ is the real part of the complex impedance, ω is the angular frequency the perturbing ac signal and $|Z(\omega)|$ is the modulus of the impedance.

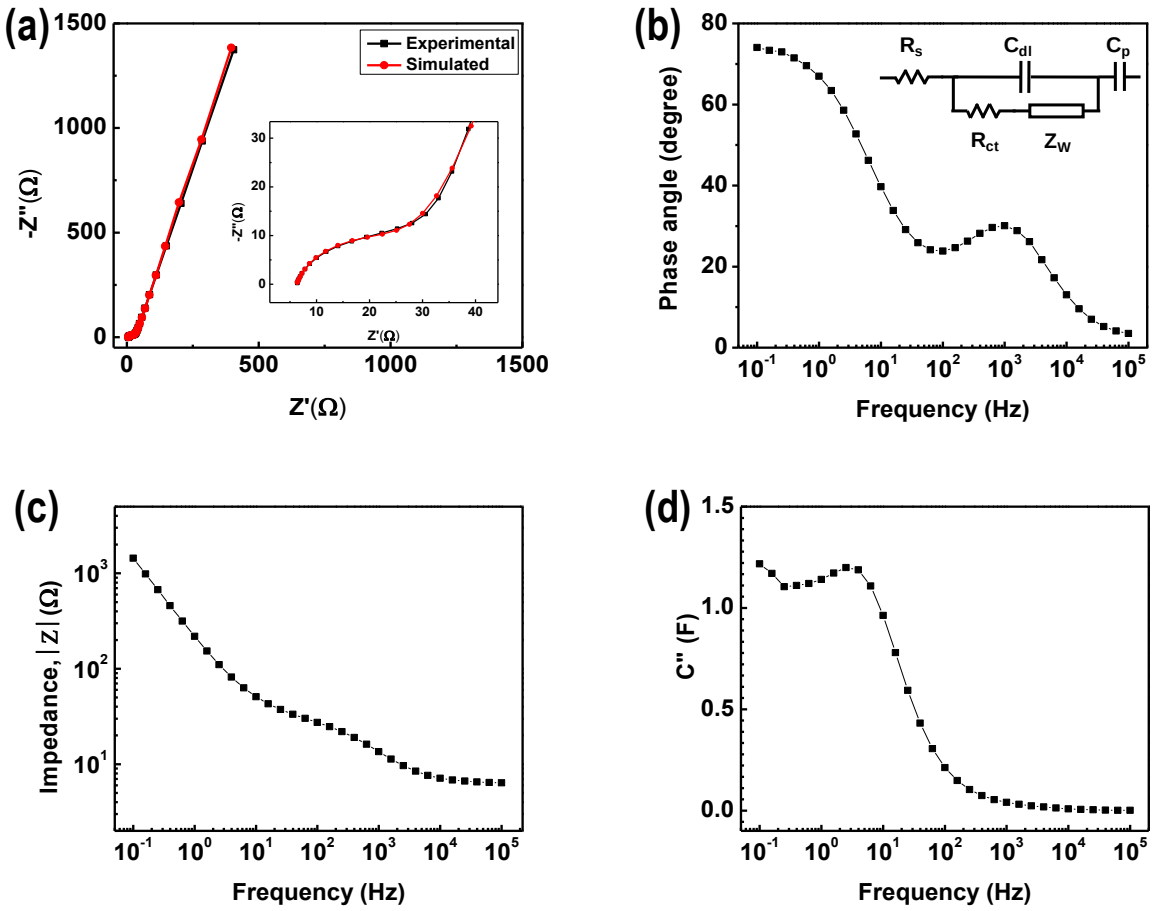

Fig. 8 Electrochemical impedance studies of the asymmetrical supercapacitor based on AC‖AC- NiO NFs performed in the frequency range of 100 kHz to 0.1 Hz at an ac amplitude of 5 mV in 6 M KOH aqueous electrolyte. (a) Experimental and simulated Nyquist plot measured with the expanded view of high frequency region in the inset; (b) Bode plot of phase angle vs. frequency and the inset shows the equivalent circuit of the asymmetric supercapacitor; (c) Bode plot of impedance vs. frequency and (d) Evolution of imaginary capacitance with frequency for the asymmetric supercapacitor.

The frequency at which maximum capacitance could be delivered is the response frequency (knee frequency) of the supercapacitor (f_0) and is 6 Hz. The response frequency divides the capacitive ($f < f_0$) and resistive ($f > f_0$) range of the suercapacitor. The corresponding relaxation time constant (or supercapacitor figure of merit, $\tau_o = 1/f_0$) of the ASC is 167 ms. The smaller time constant indicates the faster discharge of the entire stored energy of the supercapacitor which justifies the higher power density of the ASC.[42]

Conclusion

Simple and cost effective electrospinning has been carried out for the synthesis of large aspect ratio nanofibers of NiO which was composed of densely packed hexagonal nanoparticles. An asymmetric supercapacitor was designed using the NiO NF – activated carbon composite as cathode and activated carbon as anode materials. The device was capable of performing in the potential window 0 to 1.8 V at higher scan rates (10 mV/s), but better electrochemical stability and reversibility could be maintained at 1.5 V. The asymmetric supercapacitor delivered a remarkably high specific capacitance of 141 F/g with an energy density of 43.75 Wh kg^{-1} and power density of 7.5 kW kg^{-1}. The ASC exhibited high cycle stability with a capacitance retention of 88% and improved coulombic efficiency of 93% over 5000 galvanostatic charge discharge cycles. The relaxation time constant of the ASC was estimated to 167 ms.

Acknowledgements

Muhamed Shareef Kolathodi gratefully acknowledges the Council of Scientific and Industrial Research (CSIR), India for providing financial support in the form of fellowship and contingency grant.

References

1. B. E. Conway. *Electrochemical supercapacitors: Scientific fundamentals and technological applications*. Kluwer Academic/Plenum Publishers, New York, 1997
2. P. Simon and Y. Gogotsi, *Nat. Mater.*, 2008, 7, 845–854
3. M. Winter and R. J. Brodd, *Chem. Rev.*, 2004, 104, 4245–4269
4. J. R. Miller and P. Simon, *Science*, 2008, 321, 651–652
5. P. J. Hall, M. Mirzaeian and S. I. Fletcher, *Energy Environ. Sci.*, 2010, 3, 1238–1251
6. Q. Wang, Z. Wen and J. Li, *Adv. Funct. Mater.*, 2006, 16, 2141-2146
7. Y. Liang, F. Liang, H. Zhong, Z. Li, R. Fu and D. Wu, *J. Mater. Chem. A*, 2013, 1, 7000–7005
8. D. Rochefort and A. L. Pont, *Electrochem. Commun.*, 2006, 8, 1539–1543
9. H. Q. Wang, Z. S. Li, Y. G. Huang, Q. Y. Li and X. Y. Wang, *J. Mater. Chem.*, 2010, 20, 3883–3889
10. J. Zhang, J. Jiang, H. Li and X. S. Zhao, *Energy Environ. Sci.*, 2011, 4, 4009–4015
11. F. Wang, S. Xiao, Y. Hou, C. Hu, L. Liu and Y. Wu, *RSC Adv.*, 2013, 3, 13059–13084
12. B. G. Choi, S.-J. Chang, H.-W. Kang, C. P. Park, H. J. Kim, W. H. Hong, S. Lee and Y. S. Huh, *Nanoscale*, 2012, 4, 4983–4988
13. Y.-G. Wang, Z.-D. Wang and Y.-Y. Xia, *Electrochim. Acta*, 2005, 50, 5641-5646
14. C. Peng, S. Zhang, X. Zhou and G. Z. Chen, *Energy Environ. Sci.*, 2010, 3, 1499–1502
15. G. P. Wang, L. Zhang and J. J. Zhang, *Chem. Soc. Rev.*, 2012, 41, 797–828
16. K. C. Liu and M. A. Anderson, *J. Electrochem. Soc.*, 1996, 143, 124–129
17. C. Z. Yuan, X. G. Zhang, L. H. Su, B. Gao and L. F. Shen, *J. Mater. Chem.*, 2009, 19, 5772–5777
18. S. Ding, T. Zhu, J. S. Chen, Z. Wang, C. Yuan and X. W. Lou, *J. Mater. Chem.*, 2011, 21, 6602-6606
19. Z. Y. Ji, X. P. Shen, Y. L. Xu, H. Zhou, S. Bai and G. X. Zhu, *RSC Adv.*, 2014, 4, 13601–13609
20. S. Cheng, L. Yang, Y. Liu, W. Lin, L. Huang, D. Chen, C. P. Wong and M. Liu, *J. Mater. Chem. A*, 2013, 1, 7709–7716
21. M. S. Wu, Y. R. Zheng, G. Lin, *Chem. Commun.*, 2014, 50, 8246– 8248

22. K. Anandan and V. Rajendran, *Mater. Sci. Semicond. Process*, 2011, 14, 43-47
23. Y. Zhang and Z. Guo, *Chem. Commun.*, 2014, 50, 3443–3446
24. D. H. Reneker and I. Chun, *Nanotechnology*, 1996, 7, 216-223
25. Z.-M. Huang, Y.-Z. Zhang, M. Kotaki and S. Ramakrishna, *Compos. Sci. Technol.*, 2003, 63, 2223–2253
26. J. T. McCann, D. Li and Y. N. Xia, *J. Mater. Chem.*, 2005, 15, 735-738
27. M. Y. Song, D. K. Kim, K. J. Ihn, S. M. Jo and D. Y. Kim, *Nanotechnology*, 2004, 15, 1861-1865
28. C. T. Cherian, J. Sundaramurthy, M. Kalaivani, P. Ragupathy, P. S. Kumar, V. Thavasi, M. V. Reddy, C. H. Sow, S. G. Mhaisalkar, S. Ramakrishna and B. V. R. Chowdari, *J. Mater. Chem.*, 2012, 22, 12198–12204
29. G. Wee, H. Z. Soh, Y. L. Cheah, S. G. Mhaisalkar and M. Srinivasan, *J. Mater. Chem.*, 2010, 20, 6720–6725
30. S. Cavaliere, S. Subianto, I. Savych, D. J. Jones and J. Roziere, *Energy Environ. Sci.*, 2011, 4, 4761–4785
31. D. W. Wang, F. Li and H. M. Cheng, *J. Power Sources*, 2008, 185, 1563–1568
32. C. Z. Yuan, X. G. Zhang, Q. F. Wu and B. Gao, *Solid State Ionics*, 2006, 177, 1237–1242
33. C. Z. Yuan, B. Gao and X. G. Zhang, *J. Power Sources*, 2007, 173, 606-612
34. H. Wang, H. Yi, X. Chen and X. Wang, *J. Mater. Chem. A*, 2014, 2, 3223-3230
35. F. Luan, G. Wang, Y. Ling, X. Lu, H. Wang, Y. Tong, X.-X. Liu and Y. Li, *Nanoscale*, 2013, 5, 7984-7990
36. S. Mohan, P. Srivastava, S. N. Maheshwari, S. Sundar and R. Prakash, *Analyst*, 2011, 136, 2845-2851
37. R. E. Dietz, G. I. Parisot and A. E. Meixner, *Phys. Rev. B: Solid State*, 1971, 4, 2302-2310
38. Md. A. Ali, P. R. Solanki, M. K. Patel, H. Dhayani, V. V. Agrawal, R. John and B. D. Malhotra, *Nanoscale*, 2013, 5, 2883-2891
39. S. J. Azhari and M. A. Diab, *Polym. Degrad. Stab.*, 1998, 60, 253-256
40. G. A. M. Hussein, A. K. H. Nohman and K. M. A. Attyia, *J. Therm. Anal.*, 1994, 42, 1155-1165

41. J. C. De Jesus, I. González, A. Quevedo and T. Puerta, *J. Mol. Catal. A: Chem.*, 2005, 228, 283–291

42. P. L. Taberna, P. Simon and J. F. Fauvarque, *J. Electrochem. Soc.*, 2003, 150, A292–A300

Electrospun NiO nanofibers as cathode materials of high performance asymmetric supercapacitors

Muhamed Shareef Kolathodi, Milan Palei and Tirupattur Srinivasan Natarajan*

Conducting Polymer Lab, Department of Physics, Indian Institute of Technology Madras, Chennai - 600036, India Fax: +91- 44 22574852; Tel: +91- 4422574860;

Email: tsn@.iitm.ac.in

Graphical abstract

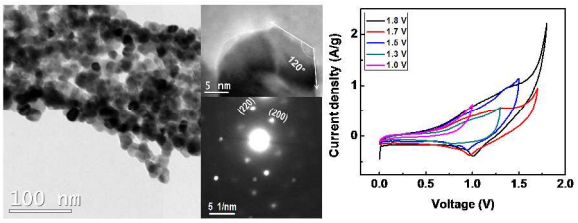

Highly granulated NiO nanofibers were prepared by electrospinning and investigated their electrochemical properties as cathode materials for asymmetrical supercapacitors.